Chapter 5

The Correlation of UVX QSOs with Foreground Galaxy Clusters

5.1 Introduction

The existence of associations between high redshift QSOs and low redshift galaxies has been controversial for a number of years; by some this association has been taken as evidence of the non-cosmological nature of QSO redshifts (Hoyle & Burbidge, 1996). However, there are more popular explanations which have been offered, that reconcile the observations with the standard cosmological world view. In particular, gravitational lensing can give a natural explanation for an association that is real but not physical; statistical lensing can be invoked to produce an excess or deficit in QSO counts around a particular lens. An excess can be produced in a flux limited sample because objects intrinsically fainter than the flux limit can be amplified and hence artificially added to the sample (Gott & Gunn, 1974). As lensing also produces a distortion in the expected 2-D image, reducing the real background area observed, a deficit in the number of background objects can also arise (Wu, 1994) if the intrinsic number-count slope of the source objects is sufficiently flat. Although it is hard to imagine other mechanisms which would produce an excess of QSOs near low redshift galaxies or galaxy clusters, this is not the case with anti-correlations. Dust in the intervening object could produce a deficit, though observations of galaxy groups and clusters do not show the presence of significant amounts of dust (Ferguson, 1993).

If correct, the lensing hypothesis allows important constraints to be placed on cosmology and large-scale structure. The excess or deficit of QSOs near a cluster can be used to weigh the cluster. This method has the advantage over other mass estimates in that it allows a measurement of the absolute mass of the cluster, while other estimators such as the measurement of velocity dispersions and the observation of shear due to strong lensing are effectively measuring the gradient of the cluster potential. Thus, in principle, it is possible to determine directly the fractional mass over-density of a cluster by comparing mass estimates from amplification by weak lensing and from shear by strong lensing. In practice the QSO density is too low to determine the mass for individual clusters (although faint galaxy counts may be able to do this) and so we use large samples of clusters to obtain a statistical measure of the mass in the cluster population.

There is a large amount of observational evidence for QSO-galaxy associations, a selection of results being given in Table 1 of Wu (1994). Most find a positive association of QSOs with foreground galaxies, using samples of bright QSOs (e.g. Tyson, 1986). In this Chapter we will first investigate the anti-correlation between faint UVX objects and galaxy clusters and groups found by Boyle et al., (1988) (BFS88), (see also Shanks et al., 1983). We shall then go on to use the 2dF QSO Survey UVX catalogue (Chapter 4) and the Abell-Corwin-Olowin (ACO) (Abell et al., 1989) and APM (Dalton et al., 1997) galaxy cluster catalogues to extend this investigation. In Chapter 2 we commented on the possible contribution of gravitational lensing to the correlation of faint galaxies and QSOs while trying to determine QSO environments. In this Chapter we will determine the level of this effect to ascertain whether gravitational lensing has any effect on the conclusions of Chapter 2. Finally we will discuss the cosmological implications of the results in our conclusions. However, first, we review some of the theoretical aspects of gravitational lensing, and discuss the components of the lensing models used.

5.2 Statistical Gravitational Lensing

Gravitational lensing is caused by the deflection of photons by large masses; the deflection angle, α, is given by

$$\alpha = \frac{4GM(<b)}{bc^2} = \frac{D_{\rm s}}{D_{\rm ls}}(\theta - \theta_{\rm q}) \tag{5.1}$$

where α, b, θ and θ_q are defined in Fig. 5.1 and D_s, D_l and D_{ls} are the angular diameter distances from the observer to the source, the observer to the lens and the lens to the source respectively (also shown in Fig. 5.1). $M(<b)$ is the mass contained within a radius b of the lens centre. Surface brightness is conserved, which implies the images will be amplified by a factor, A, which is defined by

$$A = \left|\frac{\theta}{\theta_{\rm q}}\frac{{\rm d}\theta}{{\rm d}\theta_{\rm q}}\right| \tag{5.2}$$

(Turner et al., 1984). A graphical representation of this is shown in Fig. 5.2. Clearly the amplification depends on the form of the mass distribution. We use two analytic mass profiles; the first, and simplest, of these being the single isothermal sphere (SIS), which has a mass surface density, Σ, defined by

$$\Sigma_{\rm SIS} = \frac{\sigma^2}{2Gr} \tag{5.3}$$

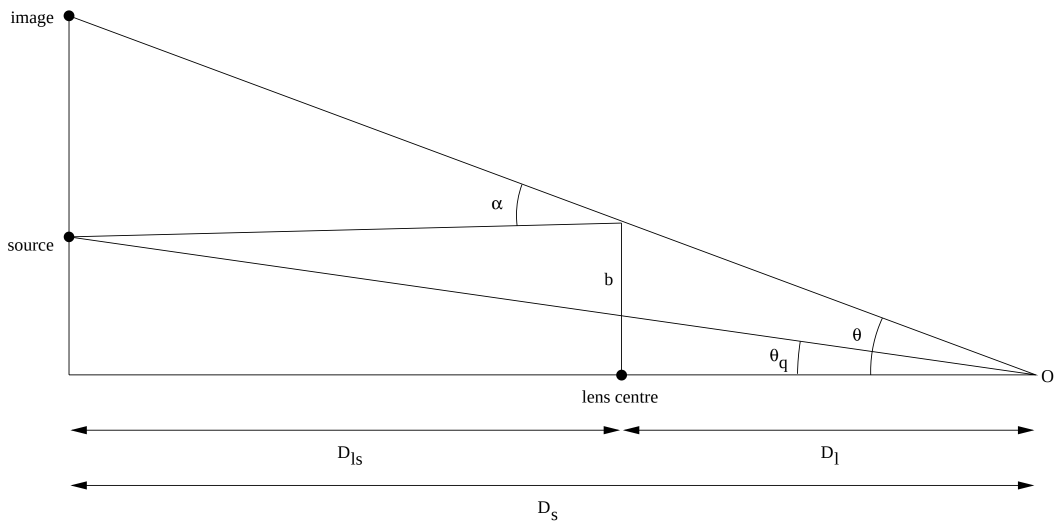

Figure 5.1: The geometry of gravitational lensing; light from the un-lensed source, which passes the lensing mass at a distance b, is deflected by an angle α into the line of sight of the observer.

where σ is the 1-D velocity dispersion of the isothermal sphere. When integrated from $r = 0$ to $r = b$ this gives

$$\alpha = 4\pi \frac{\sigma^2}{c^2} \tag{5.4}$$

which when combined with Eqs. 5.1 and 5.2 gives amplification as a function of θ,

$$A = \frac{\theta}{\theta - \theta_{\rm E}}, \qquad \theta > \theta_{\rm E} \tag{5.5}$$

where $\theta_{\rm E}$ is the Einstein radius, the radius within which multiple images can occur. For the SIS case this is

$$\theta_{\rm E} = 4\pi \frac{D_{\rm ls}}{D_{\rm s}} \left(\frac{\sigma}{c}\right)^2 \tag{5.6}$$

In our second mass profile we add a uniform density plane to the isothermal profile (SIS+plane). This is a good approximation to the effects of clustering and large scale structure (as pointed out by Wu et al., 1996), because a distribution of isothermal spheres with an auto-correlation function of the form $\xi(r) \sim r^{-2}$ produces a uniform mass surface density. The true auto-correlation function slope is ~ -1.8, which produces a sheet of matter which is uniform to better than 10%. The total surface density then becomes

$$\Sigma = \Sigma_{\rm c} + \frac{\sigma^2}{2Gr} \tag{5.7}$$

where $\Sigma_{\rm c}$ is the mass surface density in the uniform plane. This mass distribution produces the amplification

$$A = \frac{\theta}{\theta - \theta_{\rm E}(1 - \Sigma_{\rm c}/\Sigma_{\rm crit})} \frac{1}{(1 - \Sigma_{\rm c}/\Sigma_{\rm crit})^2} \tag{5.8}$$

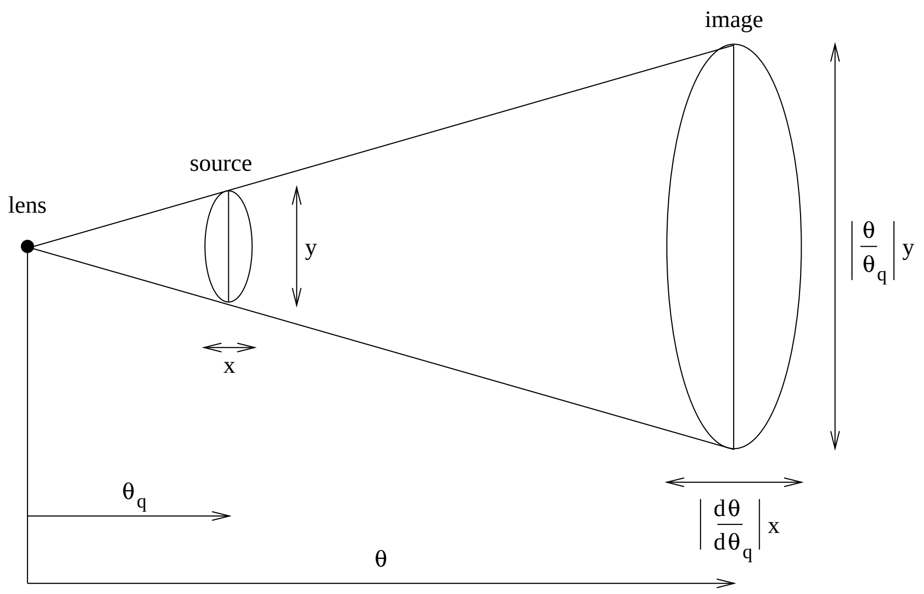

Figure 5.2: The amplification due to gravitational lensing; surface brightness is conserved to give the image a greater total brightness which depends on the distance that the image has been deflected.

where the critical surface density, $\Sigma_{\rm crit}$, is the average surface density required to create multiple images,

$$\Sigma_{\rm crit} = \frac{D_{\rm s}c^2}{D_{\rm ls}D_{\rm l}4\pi G} \tag{5.9}$$

We now come to the question of how this amplification affects the relative distributions of lenses and sources. Looking at this problem from a statistical point of view, we see that it is possible for gravitational lensing to cause an over- or under-density of source objects near to the lens. The ratio of observed surface density to the true surface density (un-lensed) is the enhancement factor, q, given by

$$q = \frac{N(< m + 2.5\log(A))}{N(< m)}\frac{1}{A} \tag{5.10}$$

(Narayan, 1989), where A is the amplification factor and $1/A$ is the effective area distortion. $N(< m)$ is the integrated number count of source objects brighter than magnitude m. It is therefore obvious that the enhancement factor is strongly dependent on the form of the integrated number count. If we take a power law form for the counts, say $N(< m) \propto 10^{\beta m}$, the enhancement is given by

$$q = \frac{1}{A}\frac{10^{\beta(m+2.5\log(A))}}{10^{\beta m}} = A^{2.5\beta-1} \tag{5.11}$$

If $A > 1$ we then have

$$q \begin{cases} < 1, & \beta < 0.4 \\ = 1, & \beta = 0.4 \\ > 1, & \beta > 0.4 \end{cases} \tag{5.12}$$

so q depends only on the amplification and the slope of the integrated source number count. We can then associate the enhancement factor q with the angular cross-correlation function $\omega(\theta)$. This gives

$$\omega(\theta) = q - 1 = A^{2.5\beta-1} - 1 \tag{5.13}$$

5.3 The Correlation of Durham/AAT QSOs and Galaxy Clusters

We first look at the result from the Durham/AAT UVX Survey (Boyle, 1986; Boyle et al., 1990) which shows an anti-correlation between UVX QSO candidates and galaxy clusters (BFS88). This cross-correlation was carried out within 7 UKST fields, using COSMOS scans of photographic plates. Three of these also had emission line objects selected from objective prism plates and two other fields contained only emission line selected objects. Extensive spectroscopy of the UVX catalogue (Boyle et al., 1987) suggested that with a colour limit of $u' - b < -0.4$ there was ~ 55 per cent contamination by Galactic stars. In the UVX sample used, the $u' - b$ selection criterion was tightened to $u' - b < -0.5$, reducing this contamination to 25 per cent while keeping 85 per cent of the spectroscopically identified QSOs. The UVX catalogue was then split into two magnitude limited samples, $17.9 < b < 19.9$ (bright) and $17.9 < b < 20.65$ (faint). The galaxy catalogue consists of all galaxies to a limit of $b_J = 20.0$ and the cluster sample was created using a multiplicity algorithm (Gott & Turner, 1977; Stevenson, 1985). Groups of seven or more galaxies with density greater than 8 times the average for the field were classed as clusters, which amounted to 10 per cent of the total number of galaxies. The emission line catalogue was taken from various sources (Savage & Bolton, 1984; Clowes & Savage, 1983; Chen, 1984; Savage et al., 1984). Cross-correlation was carried out between the entire galaxy catalogue and the UVX sample but no correlation was found on any scale. Cross-correlation of cluster galaxies with the UVX catalogue resulted in negative correlations on scales $< 5'$ for both the bright and faint samples, the bright sample showing a marginally more negative clustering signal. This can be interpreted as due to the decrease in contamination from the smaller photometric errors at brighter magnitudes. A negative correlation was also found between the emission line objects and the cluster galaxies; however, we will not discuss the emission line catalogue any further as the selection process used (objective prism plates) may tend to introduce negative correlations with dense regions.

5.3.1 A comparison of lensing models and the data

The effect of gravitational lensing is strongly dependent on the slope of the QSO number-magnitude relation at faint magnitudes. We use the number counts from Boyle, Shanks & Peterson (1988) which give a faint end slope of $\simeq 0.28$. A flatter slope would reduce the lensing mass required. The separation of observer, lens

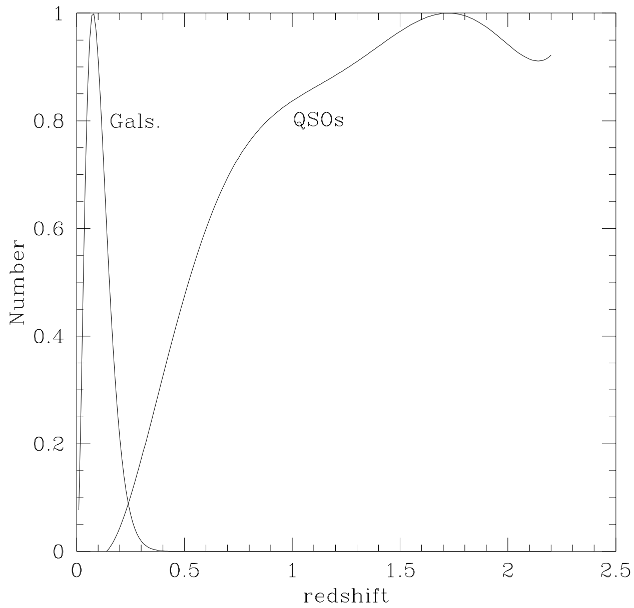

Figure 5.3: Redshift distributions assumed for the galaxy and QSO populations in the lensing models described in the text. The normalizations of the two curves are arbitrary.

and source also affects the lensing amplification. To take this into account in our model, we integrate the known QSO redshift distribution over the effective range of the Durham/AAT survey ($0.3 < z < 2.2$). This gives us an effective lensing amplification for a particular lens mass. For the galaxies we assume the analytic form of $N(z)$ given by Baugh & Efstathiou (1993):

$$\frac{\mathrm{d}N}{\mathrm{d}z} \propto z^2 \exp\left[-\left(\frac{z}{z_{\mathrm{c}}(m)}\right)^{3/2}\right] \tag{5.14}$$

where $z_{\mathrm{c}} = (0.016(b_{\mathrm{J}} - 17.0)^{1.5} + 0.046)/1.412$. This is shown integrated to $b_{\mathrm{J}} = 20$ in Fig. 5.3 along with a polynomial fit to the QSO $N(z)$. It is clear from this plot that the two populations occupy almost completely independent volumes, less than 1% of the QSOs are at $z < 0.3$ while less than 0.5% of the galaxies are at $z > 0.3$. We assume an $\Omega_0 = 1$ cosmology throughout this analysis, but it should be noted that when the lensing mass is at low redshift ($z \sim 0.1$) cosmology has a relatively small effect as $D_{\mathrm{s}} \sim D_{\mathrm{ls}}$.

We compare the SIS lens model (from Eqs. 5.5 and 5.13) to the cross-correlation results from the faint sample. Using a minimum χ^2 fit the velocity dispersion is $\sigma = 1165^{+76}_{-90}\mathrm{kms}^{-1}$ (reduced $\chi^2 = 1.40$). The equivalent Einstein radius for the fit is $0.58'$. The dotted line in Fig. 5.4 shows this model. The two component SIS+plane model (Eqs. 5.8 and 5.13) is shown as the dashed line in Fig. 5.4, the best fit in this case has velocity dispersion $\sigma = 1063^{+110}_{-142}\mathrm{kms}^{-1}$ (the equivalent Einstein radius for this is $0.46'$) and the surface density in the plane of $\Sigma_{\mathrm{c}} = 0.0569 \pm 0.0238h$ g cm^{-2}. The reduced χ^2 for this fit is 1.07. The confidence levels for this fit are shown in Fig. 5.5. As discussed above, even with an extreme $U - B$ selection there will be $\sim 25\%$ contamination. Allowing for this contamination in our models, assuming

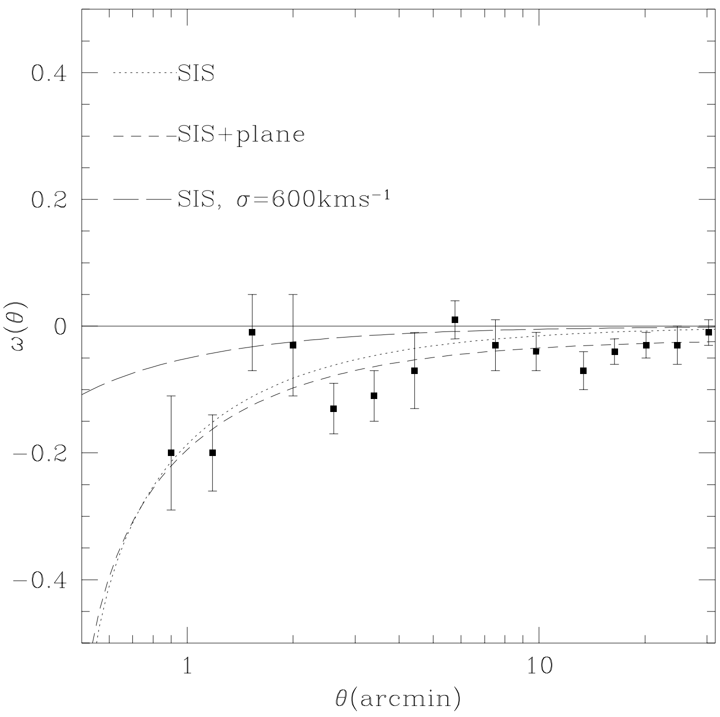

Figure 5.4: UVX-cluster cross-correlation for the faint UVX sample of BFS88 showing the best fit models; the dotted line shows the best fit single isothermal sphere model ($\sigma = 1165^{+76}_{-90}$kms^{-1}), while the dashed line shows the isothermal sphere plus constant density plane. The long-dashed line shows a lensing SIS model with $\sigma = 600$kms^{-1}.

that the cross-correlation between the stellar contamination and the galaxy clusters is zero, we find that the best fit parameters are increased. For the SIS model we find $\sigma = 1286^{+72}_{-91}$kms^{-1}, and for the two component model $\sigma = 1205^{+85}_{-108}$kms^{-1} and $\Sigma_c = 0.0779 \pm 0.0232h$ g cm^{-2}. Confidence contours for this fit are also shown in Fig. 5.5.

The values found are significantly larger than directly measured velocity dispersions of poor clusters and groups. However, because BFS88 correlate cluster members with UVX objects, they effectively weight each cluster by the number of member galaxies. Stevenson et al., (1988) find the fraction of clusters, defined using the multiplicity algorithm, as a function of the number of members, which is an approximate power-law with a slope of -2.2. From this we can calculate the mean cluster membership, $\bar{n}$. Integrating the relationship between $n = 7$ and $n = 50$ gives $\bar{n} = 15$. However, we should also weight this mean by the number of members; when this is done, $\bar{n} = 20$. Thus, the BFS88 result is probing clusters which typically have ~ 20 members. The density on the sky of these clusters is ~ 0.8 deg^{-2}, which can be compared to the density of clusters in the APM Cluster Catalogue (Dalton et al., 1997, also see Section 5.4 below) of ~ 0.2 deg^{-2} and the density of richness class 0 or greater Abell clusters which is ~ 0.1 deg^{-2} (Abell et al., 1989). Thus an 'average' cluster used by BFS88 is significantly poorer than Abell richness clusters. In this context it appears that the velocity dispersions found assuming the lensing

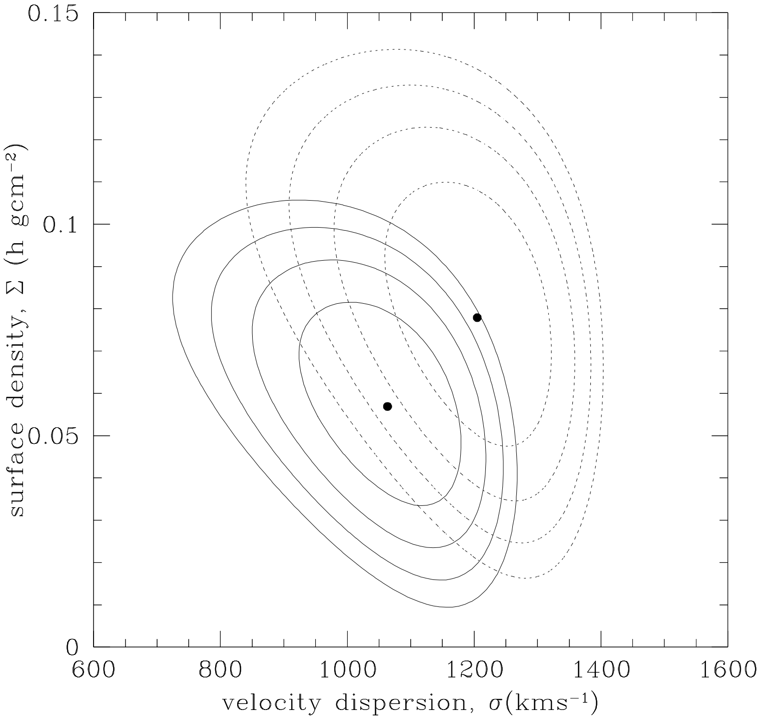

Figure 5.5: Confidence contours for the fit of the two component SIS+plane model to the cross-correlation result for the faint UVX sample. The solid contours show the results uncorrected for contamination, while the dotted lines are corrected for 25% stellar contamination. Contours are at $\Delta\chi^2 = 1, 2, 3, 4$.

models were too large, and we can make a similar argument in the case of the matter density in the uniform plane. Wu et al., (1996) find that the maximum mass likely to be associated with lenses from large-scale structure is $\sim 0.01 - 0.02h$ g cm^{-2}, which assumes that the matter density in clusters is near the critical density (i.e. $\Omega_{\rm clus} \sim 1$). A more conventional velocity dispersion for clusters of this richness is $\sigma \sim 600$kms^{-1}. The lensing model corresponding to this velocity dispersion is plotted in Fig. 5.4. Although this model is formally rejected at $> 5\sigma$, a possible error in the normalization of the BFS88 data on large scales, so that the real $\omega(\theta)$ was zero on $\sim 10'$ scales, would bring the low velocity dispersion model into agreement with the data.

BFS88 originally interpreted the UVX QSO-cluster anti-correlation as being due to absorption by dust present in clusters, the required amount of absorption being $A_{\rm B} \simeq 0.2$ mag. Ferguson (1993) used the relation between the $\rm Mg_2$ index and $B-V$ colours for a large sample of elliptical galaxies in clusters to determine the reddening due to dust in these clusters. He finds no evidence for any reddening, and the 90% upper limit on the reddening is $E(B-V) = 0.06$, an upper limit which is just consistent with the required absorption, assuming $A_{\rm B} = 4.10E(B-V)$. It could be argued that dust is more likely to survive in poorer clusters and groups as the temperature of the intra-cluster medium will be lower. However, Ferguson finds no evidence for reddening in group environments either. Given the upper limits on dust in clusters, it is still possible that lensing and absorption could both play a part in the anti-correlation found. The cluster masses estimated from statistical lensing might then be brought into line with other estimates.

5.4 The Correlation of 2dF UVX QSOs and Rich Clusters

5.4.1 The data and methods

To further test the lensing hypothesis we turn to a much larger UVX sample, the candidate list for the 2dF QSO redshift survey which was discussed in detail in Chapter 4. This catalogue consists of $\sim$ 46000 UVX QSO candidates covering an area of 740 $\deg^2$ in the magnitude range $18.25 < b_J < 21.0$. We use a bluer UVX selection than is used for the full QSO survey in order to reduce the level of contamination, $u - b_J \leq -0.5$ leaves only 25% contamination (estimated from the preliminary spectroscopic observations in Chapter 6) and a total of $\sim$ 30000 UVX objects.

We use two galaxy cluster catalogues which overlap our fields: the first is the ACO catalogue (Abell et al., 1989) which has 44 clusters within the bounds of the Northern strip and 158 clusters in the Southern strip (including the 'supplementary Southern clusters') which are richness class 0 or greater. The second sample is the APM Cluster Survey (Dalton et al., 1997) which has 59 clusters in the area of the Southern strip. The ACO catalogue was constructed on the basis of visual inspection of photographic plates and is therefore prone to systematic errors which are largely unquantifiable. This could cause potential problems if the errors introduce spurious clusters into the sample; so by also selecting clusters on the basis of richness we hope to reject the majority of these spurious clusters. The APM sample is selected using an automated algorithm from the APM Galaxy Survey (Maddox, 1988), so any contamination by spurious clusters is likely to be smaller and more uniform. Of course, we should also note that the cluster catalogue used in the BFS88 analysis is a catalogue of poorer clusters, and so more prone to contamination by chance alignments of galaxies along the line-of-sight. All the APM clusters have estimated distances from the photometry of member galaxies and $\sim$ 100 have reliable redshift determinations, which allows us to determine the cross-correlation function as a function of projected proper distance as well as angular distance. Table 5.1 contains the numbers of clusters within the two 2dF QSO survey strips at different richness levels. Different richness parameters are used in the APM and ACO samples. Fig 5.6 shows both the distribution of UVX objects with $u - b_J \leq -0.5$ and the positions of the clusters used in this analysis.

The cross-correlation function was estimated in the standard manner, using the estimator in Eq. 2.1, counting the number of UVX objects and random points a distance $\theta \pm \delta\theta/2$ from the cluster centres. The random points were distributed

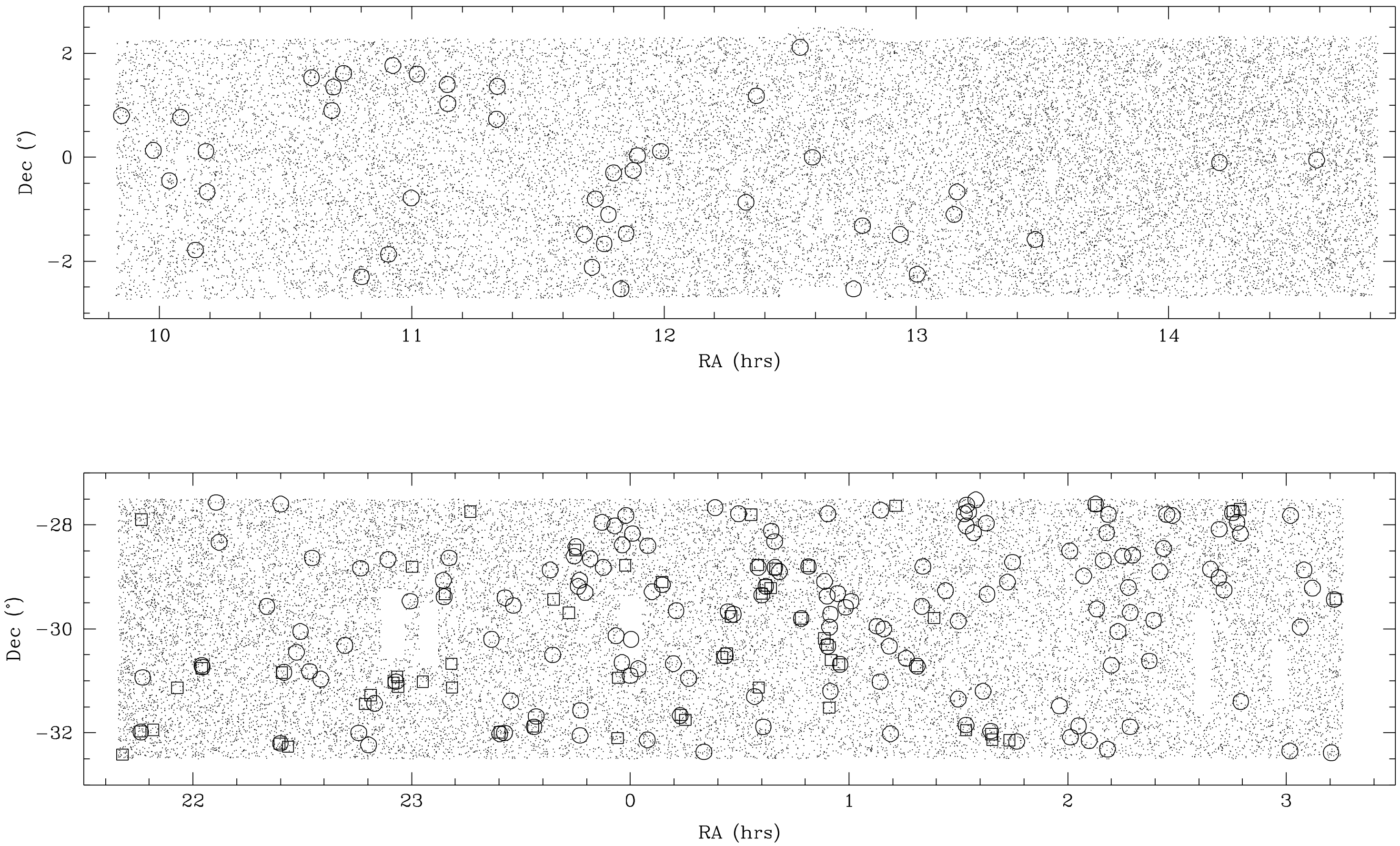

Figure 5.6: The 2dF UVX catalogues for the Northern ($\delta = 0°$) and Southern ($\delta = -30°$) strips with $18.25 \leq b_{\rm J} \leq 21.0$ and $u - b_{\rm J} \leq -0.5$. Open circles show the positions of ACO clusters while open squares show the positions of APM clusters. Note that the declination axis has been expanded in order to make these plots clearer.

Table 5.1: Details of the cluster samples used in the cross-correlation analysis with 2dF UVX objects, showing the number of clusters for different richness selections. Note that the APM sample uses a different richness criterion.

Cluster Sample	No. of Clusters $R_{\rm ACO} \geq 0$	$R_{\rm ACO} \geq 1$	$R_{\rm ACO} \geq 2$
ACO South	158	71	22
ACO North	44	28	11
	$R_{\rm APM} \geq 40$	$R_{\rm APM} \geq 45$	$R_{\rm APM} \geq 50$
APM	59	41	27

uniformly within the area of the 2dF UVX sample taking into account areas removed due to bright stars and plate defects. The random point density was 25 times the UVX density.

5.4.2 Results

Before carrying out the UVX-cluster cross-correlation we first measured the cross-correlation function of all the images classified as stellar in our survey area ($17.0 \leq b_{\rm J} \leq 21.0$), with the clusters. Fig. 5.7 shows the results of this cross-correlation. We clearly see a positive signal of amplitude ~ 0.05 from $\sim 1'$ to $40'$. Some fraction of this signal may be due to contamination of the stellar catalogue by galaxies. By comparing the amplitude of this clustering to the cluster-galaxy correlation function, we estimate that there is a possible $\sim 10 - 15\%$ contamination in the catalogue. In Chapter 6 we find that spectroscopic follow up of the UVX catalogue identifies 16% of the sample as narrow emission line galaxies. However most of these objects are both faint and red, with $b_{\rm J} \geq 20.6$ and $u - b_{\rm J} \geq -0.5$. With $u - b_{\rm J} \leq -0.5$ and $b_{\rm J} \leq 21$ the contamination is 7.7%, while with $u - b_{\rm J} \leq -0.5$ and $b_{\rm J} \leq 20.6$ only 4.9% of the UVX candidates are galaxies. Thus, by using a blue selection with $u - b_{\rm J} \leq -0.5$ we reduce this contamination to a minimum.

The cross-correlation functions for all the clusters in each sample are shown in Fig 5.8, correlated with UVX objects in the magnitude ranges $18.25 \leq b_{\rm J} \leq 21.0$ and $20.0 \leq b_{\rm J} \leq 21.0$. Neither of the cluster samples show a significant cross-clustering signal. The aim of using a fainter sub-sample of UVX objects was to use only objects inhabiting the regime where the QSO number counts are flat. Even this sample fails to show the expected negative correlation which would be the signature of gravitational lensing. We also attempted a cross-correlation of only bright QSOs, $17 \leq b_{\rm J} \leq 19$, (including the bright candidates with $b_{\rm J} < 18.25$ from the bright extension of the 2dF QSO survey which is being observed using the FLAIR instrument), as the steep counts slope over this range should produce strong positive correlations from lensing. However, the numbers of QSOs in this magnitude range is small and the fractional contamination increases to reduce the signal, and

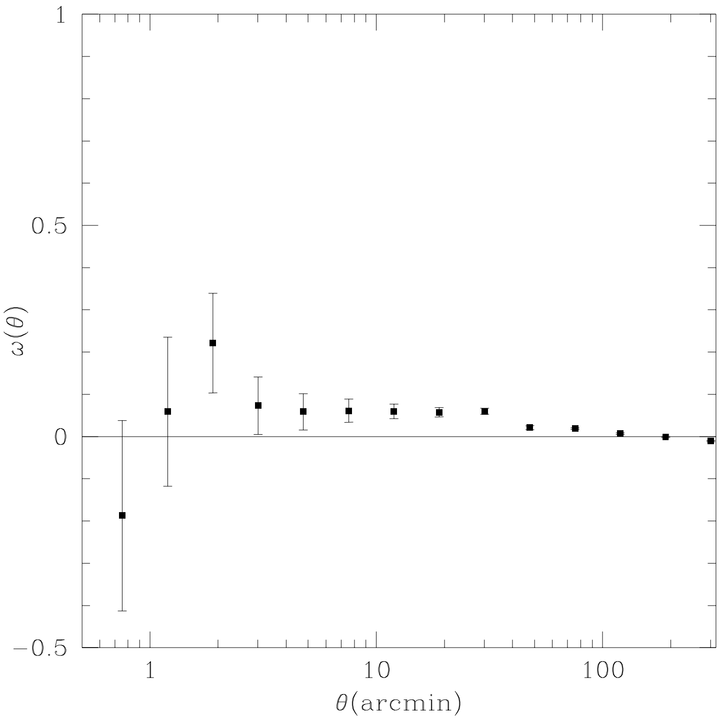

Figure 5.7: The cross-correlation function of all stellar objects ($17.0 \leq b_{\rm J} \leq 21.0$) and APM galaxy clusters in the Southern 2dF catalogue area.

no positive correlation was seen in this regime.

We next look at the cross-correlation as a function of richness, demonstrated in Fig. 5.9. The cross-correlation with APM clusters shows a marginally significant anti-correlation on scales $\sim 3 - 20'$; for $R_{\rm APM} \geq 45$ we find $\omega(\theta < 24') = -0.115 \pm 0.061$ and for $R_{\rm APM} \geq 50$, $\omega(\theta < 24') = -0.104 \pm 0.075$. The ACO sample does not show this signal, with $\omega(\theta < 24') = -0.002 \pm 0.043$ ($R_{\rm ACO} \geq 1$) and $\omega(\theta < 24') = 0.077 \pm 0.076$ ($R_{\rm ACO} \geq 2$). At angular scales greater than $30'$ the cross-correlation function is zero in all cases, thus the constant density plane lensing model cannot be consistent with these results on large scales. This might be reasonable as the model is only valid in the regime where $\xi_{\rm cc}(r) \sim r^{-2}$. At larger scales the cluster auto-correlation function turns over, producing a cut-off. Fig. 5.10 shows the projected cross-correlation function for APM clusters ($R \geq 45$), using the photometric distance estimate, which demonstrates that this cut-off is actually at $\sim 1\ h^{-1}$ Mpc, the scale of galaxy clusters, rather than $\sim 20\ h^{-1}$ Mpc which is the scale at which the power-law in the cluster-cluster auto-correlation function breaks. The clustering amplitude within $1\ h^{-1}$ Mpc in Fig. 5.10 is $\omega(r < 1\ h^{-1}\ {\rm Mpc}) = -0.197 \pm 0.078$.

An isothermal sphere profile can be fit to this data, but only the richer APM selected clusters give a significant measure of the velocity dispersion. This is $\sim 2600 \pm 1000 {\rm kms}^{-1}$ but is somewhat dependent on the range of scales fit as at small scales, close to the Einstein radius, the lensing model produces a quickly changing correlation function. Added to this problem, within the Einstein radius the model

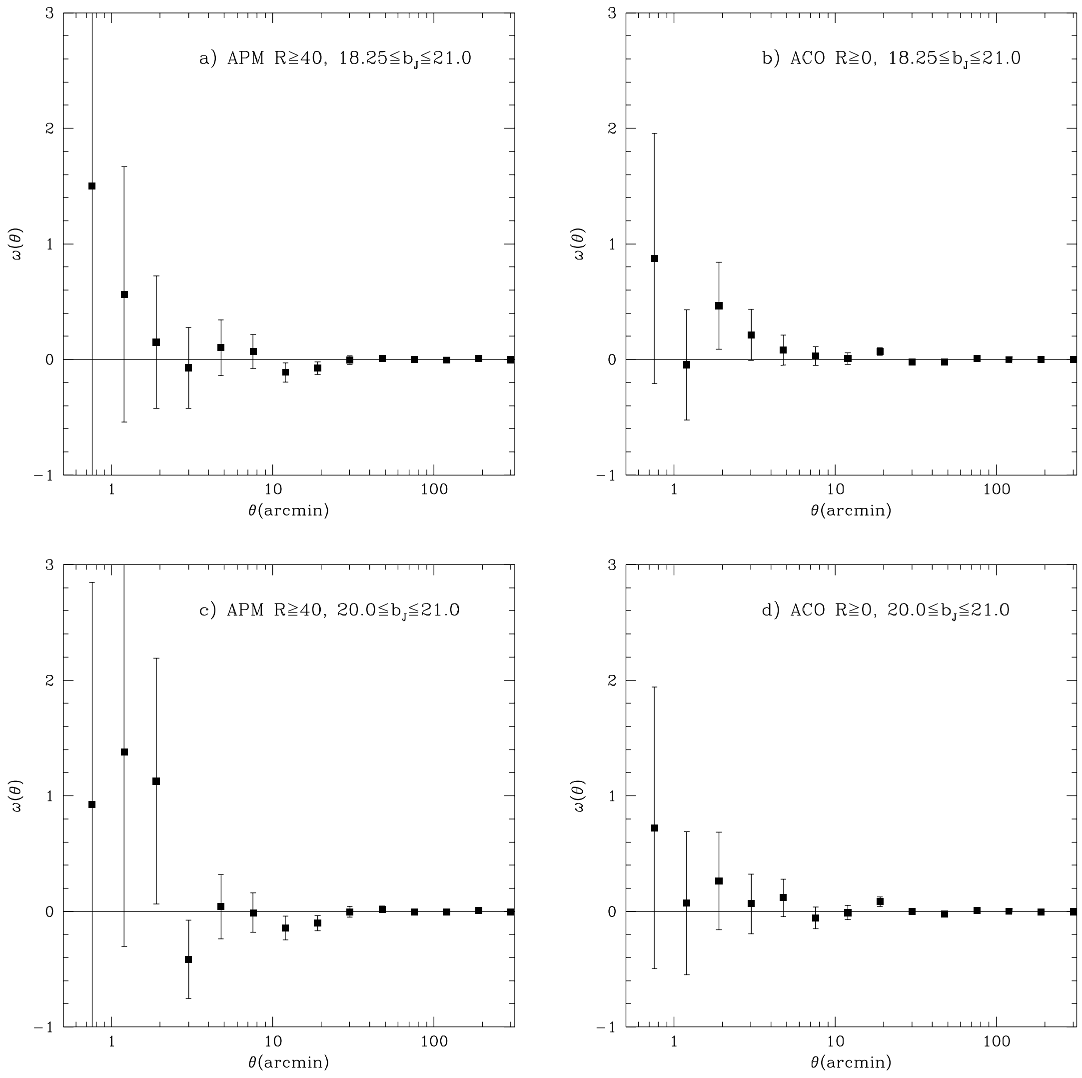

Figure 5.8: The results of angular cross-correlation between APM and ACO clusters and UVX objects ($u - b_{\rm J} \leq -0.5$). a) UVX objects in the range $18.25 \leq b_{\rm J} \leq 21.0$ and APM clusters with $R_{\rm APM} \geq 40$, b) UVX range: $18.25 \leq b_{\rm J} \leq 21.0$, ACO clusters: $R_{\rm ACO} \leq 0$, c) UVX range: $20.0 \leq b_{\rm J} \leq 21.0$, APM clusters: $R_{\rm APM} \leq 40$, d) UVX range: $20.0 \leq b_{\rm J} \leq 21.0$, ACO clusters: $R_{\rm ACO} \leq 0$.

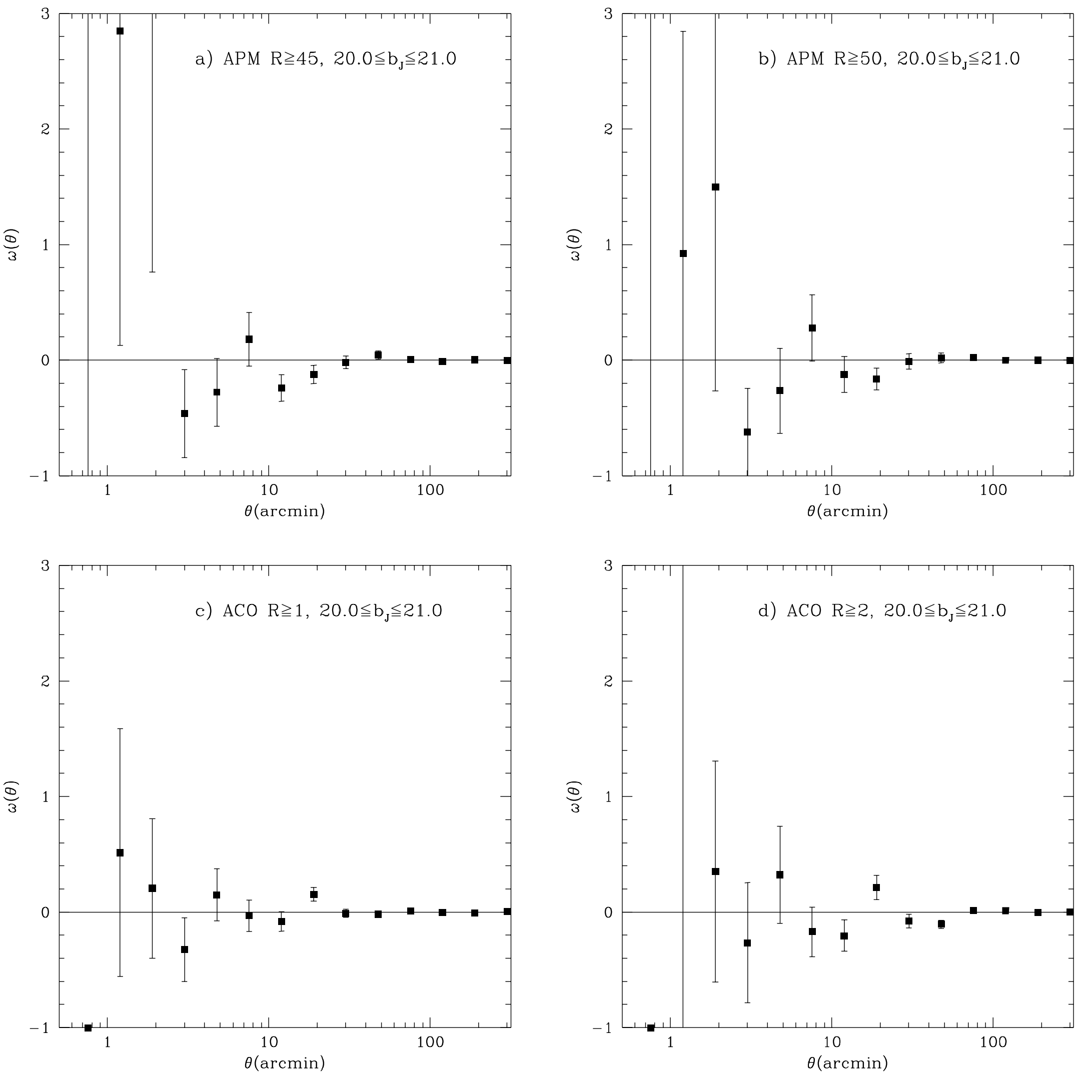

Figure 5.9: The results of angular cross-correlation between APM and ACO clusters and UVX objects ($20.0 \leq b_{\rm J} \leq 21.0$ and $u - b_{\rm J} \leq -0.5$) for a) APM $R_{\rm APM} \geq 45$, b) APM $R_{\rm APM} \geq 50$, c) ACO $R_{\rm ACO} \geq 1$ and d) ACO $R_{\rm ACO} \geq 2$.

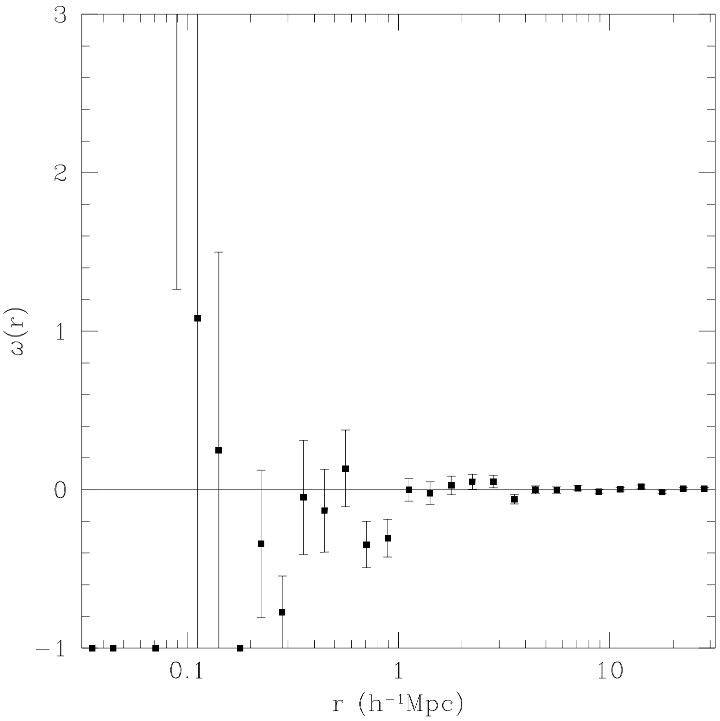

Figure 5.10: Projected cross-correlation function for UVX objects ($20.0 \leq b_J \leq 21.0$ and $u - b_J \leq -0.5$) and APM clusters $R_{APM} \geq 45$

used for the amplification is no longer valid and multiple images can be produced. It is clear from the data presented here that we cannot obtain a robust result for the correlation between rich clusters and UVX objects, which is likely to be due to the small number of cluster centres, as compared to the result of BFS88 which used individual cluster member galaxies. To demonstrate this point we show a comparison of the two data sets in Fig. 5.11. Obviously, the errors are considerably smaller in the BFS88 data.

5.5 The Correlation of QSOs and $b_J < 23$ Galaxies

Results from Chapter 2 suggested that there could be a lensing component to the cross-correlation of faint, $b_J < 23$, galaxies and optically selected QSOs, as a small anti-correlation was measured between the two populations. Here we attempt to model the effect of the lensing contribution on this result. Using the redshift distributions of the galaxy and QSO populations in Chapter 2 we construct Monte-Carlo simulations to calculate the expected correlation signal as a function of redshift. These simulations model the individual galaxy potentials as isothermal spheres, and take into account the clustering of galaxies by also adding a constant density plane as discussed above. Wu et al., (1996) calculate that the maximum matter surface density contributed by large-scale structure is $\sim 0.01 - 0.02h$ g cm^{-2} assuming that the amount of matter in galaxies is $\Omega_g \sim 1$. Typical velocity dispersions for galaxies

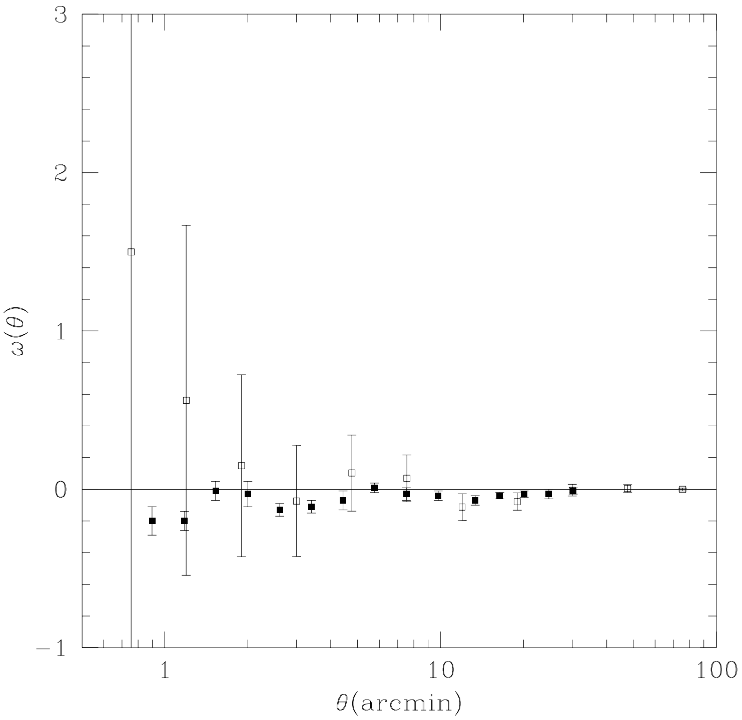

Figure 5.11: A comparison of the cross-correlation results of UVX QSOs and galaxy clusters from BFS88 and from the analysis of the 2dF UVX catalogue discussed in the text. The solid squares are the BFS88 data while the open squares are the cross-correlation of 2dF UVX candidates ($18.25 \leq b_{\rm J} \leq 21.0$) with APM clusters ($R_{\rm APM} \geq 40$).

are $\sim 200{\rm kms}^{-1}$, so we produce Monte-Carlo simulations with velocity dispersions of 200 and $400{\rm kms}^{-1}$ and constant density planes with $\Sigma = 0.0$ and $0.02h$ g cm^{-2}. Fig. 5.12 shows how the clustering amplitude in these simulations changes with redshift. The extreme case of $\Sigma = 0.02h$ g cm^{-2} and $\sigma = 400{\rm kms}^{-1}$, which can contribute ~ -0.02, can account for most of the negative signal found for QSOs at $z < 1.5$, while it cannot account for the negative correlation found at higher z. This has no effect on the rejection of high clustering amplitude models in Chapter 2, but does make the models with low clustering amplitude more consistent with the data.

5.6 Conclusions

We look at the correlation of QSOs and foreground galaxy clusters and interpret the measured anti-correlation in terms of statistical gravitational lensing. We come to the following conclusions:

1) The velocity dispersion required to fit the BFS88 result, allowing for stellar contamination in the UVX sample, is $\sigma = 1286^{+72}_{-91}{\rm kms}^{-1}$. If a uniform density sheet is added to the mass profile we require $\sigma = 1205^{+85}_{-108}{\rm kms}^{-1}$ and $\Sigma_{\rm c} = 0.0779 \pm 0.0232h$ g cm^{-2}. The velocity dispersion found is similar to that of rich galaxy

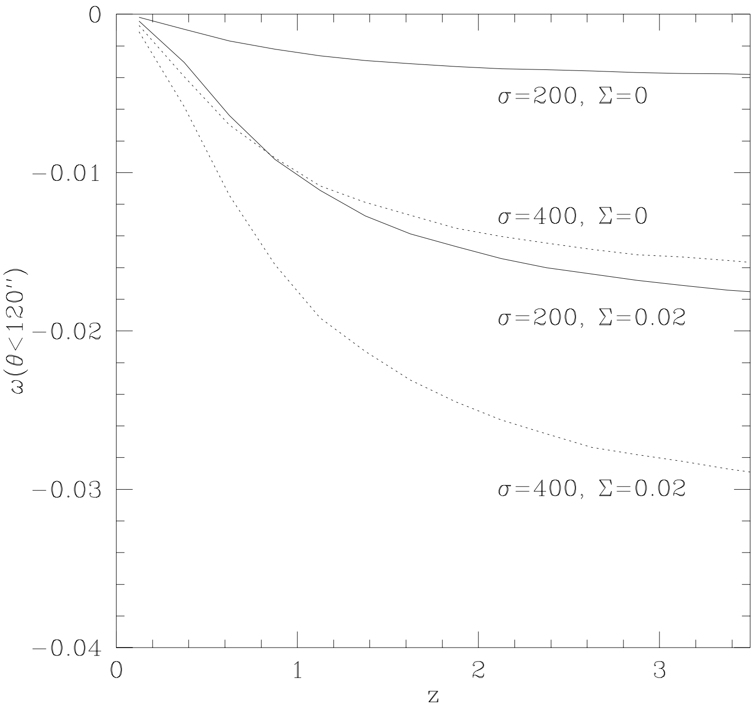

Figure 5.12: Estimated angular cross-correlation function of QSOs with faint, $b_J < 23$, galaxies due to lensing, as a function of QSO redshift. The correlation amplitude is measured within 120″ from Monte-Carlo simulations, with velocity dispersions 200 and 400kms^{-1} and planes with zero, and $\Sigma = 0.02h$ g cm^{-2} mass surface densities.

clusters, although the majority of clusters in the sample will be poor clusters so the values we find are larger than the values expected from other mass estimates. The density in the plane is larger than expected from estimates based on the known clustering properties of galaxy clusters, a value of $\sim 0.02h$ g cm^{-2} being the largest expected density in an $\Omega_0 = 1$ universe. An offset in the measured clustering at large scales ($\sim 20 - 30'$) in BFS88 would allow a more reasonable model, with $\sigma \sim 600$kms^{-1} to fit the data.

2) We test the lensing model with the 2dF UVX catalogue and the ACO and APM cluster catalogues. No significant correlation is found between the two data sets, only rich APM clusters ($R_{\rm APM} \geq 45$) and faint UVX objects show any sign of anti-correlation, although this is not strongly significant. At scales larger than ~ 1 h^{-1} Mpc the correlation function is zero in all cases. This last point does suggest that the uniform density plane is not an appropriate model to use as we would expect to see a signal on $\sim 10 - 20$ h^{-1} Mpc scales. In fact, the large planar density found using the two component model with the BFS88 data is inconsistent with the 2dF UVX/rich cluster data on these large scales.

3) The results found in Chapter 2 are not significantly affected by the inclusion of gravitational lensing. Lensing can account for most of the anti-correlation seen at low ($z < 1.5$) redshift, making a contribution of ~ -0.02. The high clustering amplitude models in Chapter 2 are still ruled out, while the low amplitude models

become more consistent with the data.

We show that it is possible to interpret the anti-correlation of QSOs and foreground clusters as an effect due to gravitational lensing. Not only this, we also find that the small anti-correlation found in Chapter 2 between QSOs and $b_{\rm J} < 23$ galaxies can be mostly explained by lensing. Generally, cluster masses predicted by the data are higher than expected from other mass estimates. Combining lensing with a small dust component in clusters could reduce the masses required to reasonable levels.

The 2dF QSO survey will produce a large homogeneous catalogue in the magnitude range $17 \leq b_{\rm J} \leq 21$, allowing a full test of the lensing hypothesis. The present stellar contamination, which is particularly dominant at bright magnitudes, combined with the relatively small number of clusters in the survey area restricts our ability to detect the characteristic features of lensing. The completed redshift survey will not have the problem of contamination, and this, combined with a variety of cluster catalogues of varying richness, will allow us to find the positive and negative signals which are the unambiguous indication of gravitational lensing.